Ureide Permease 5 (AtUPS5) Connects Cell Compartments Involved in Ureide Metabolism[1]

Ignacio Lescano,[a,2] María Florencia Bogino,[b] Carolina Martini,[a,b] Tomás María Tessi,[a] Claudio Alejandro González,[a,b] Karin Schumacher,[c] and Marcelo Desimone[a,b,3]

[a]Multidisciplinary Institute of Plant Biology, National University of Córdoba, CONICET, Vélez Sarsfield Av. 299, X5000HUA Córdoba, Argentina

[b]Plant Physiology Chair, Department of Physiology, Faculty of Exact, Physical and Natural Sciences, National University of Córdoba, Vélez Sarsfield Av. 299, X5000HUA Córdoba, Argentina

[c]Centre for Organismal Studies (COS), Heidelberg University, Im Neuenheimer Feld 230, 69120 Heidelberg, Germany

ORCID IDs: 0000-0002-1194-9508 (I.L.); 0000-0003-0565-0486 (M.F.B.); 0000-0002-5736-226X (C.M.); 0000-0001-8283-2457 (T.M.T.); 0000-0003-1763-4846 (C.A.G.); 0000-0001-6484-8105 (K.S.); 0000-0003-4382-0132 (M.D.).

Allantoin is a purine oxidative product involved in long distance transport of organic nitrogen in nodulating legumes and was recently shown to play a role in stress tolerance in other plants. The subcellular localization of enzymes that catalyze allantoin synthesis and degradation indicates that allantoin is produced in peroxisomes and degraded in the endoplasmic reticulum (ER). Although it has been determined that allantoin is mostly synthesized in roots and transported to shoots either for organic nitrogen translocation in legumes or for plant protection during stress in Arabidopsis (*Arabidopsis thaliana*), the mechanism and molecular components of allantoin export from root cells are still unknown. AtUPS5 (Arabidopsis UREIDE PERMEASE 5) is a transmembrane protein that transports allantoin with high affinity when expressed in yeast. The subcellular fate of splicing variants AtUPS5L (long) and AtUPS5S (short) was studied by tagging them with fluorescent proteins in their cytosolic loops. The capability of these fusion proteins to complement the function of the native proteins was demonstrated by nutritional and salt stress experiments. Both variants localized to the ER, but the AtUPS5L variant was also detected in the trans-Golgi network/early endosome and at the plasma membrane. AtUPS5L and AtUPS5S localization indicates that they could have different roles in allantoin distribution between subcellular compartments. Our data suggest that under nonstress conditions UPS5L and UPS5S may function in allantoin degradation for nutrient recycling, whereas under stress, both genes may be involved in vesicular export allowing allantoin translocation from roots to shoots.

The ureides allantoin and allantoic acid are the main products of the biological fixation of N_2 transported from the nodules to the shoot in tropical legumes, representing, for example, in nodulated soybean (*Glycine max*) up to 80% of the transported nitrogen (McClure and Israel, 1979; Todd et al., 2005). In other plant species, important variations in the content of ureides have been observed under different environmental conditions and developmental stages (Sagi et al., 1998; Nikiforova et al., 2005; Brychkova et al., 2008; Kanani et al., 2010; Rose et al., 2012; Ventura et al., 2014). The physiological role of this pathway and, in particular, of allantoin accumulation in non-ureide transporting species has been extensively discussed. It has been hypothesized that the pathway serves to recycle the stored nitrogen in purines when these are no longer required (Zrenner et al., 2006). However, recent studies have also shown that allantoin accumulation improves plant tolerance to different abiotic stresses (Watanabe et al., 2014; Lescano et al., 2016; Nourimand and Todd, 2016). Brychkova et al. (2008) demonstrated that ureides can modulate plant antioxidant capacity, suggesting these metabolites are potential scavengers of reactive oxygen species (ROS) produced under stress conditions. However, there is only limited and contradictory information about the reactivity of ureides against ROS (Gus'kov et al., 2002; Wang et al., 2012).

Allantoin accumulation has also been implicated in water stress tolerance in a process that involves the stress hormone abscisic acid (ABA; Watanabe et al., 2014). The mechanism proposed involves the transcriptional

[1]This work was supported by the National Fund of Science and Technology (FONCyT, Argentina) (grant no. PICT-2009-0114), the Secretary of Science and Technology of the National University of Córdoba (SECyT-UNC, Argentina), and a DAAD scholarship to perform confocal laser scanning microscopy in COS, Heidelberg, Germany (to I.L.).

[2]Senior author.

[3]Author for contact: marchelodesimone@gmail.com.

The author responsible for distribution of materials integral to the findings presented in this article in accordance with the policy described in the Instructions for Authors (www.plantphysiol.org) is: Ignacio Lescano (ignaciolescano@unc.edu.ar).

I.L. designed and performed most of the experiments, and wrote the article; M.F.B. and C.M. performed nutritional and 5-FU experiments; T.M.T. provided technical assistance to I.L.; C.A.G. and K.S. supervised the project and completed the writing; M.D. conceived the project and wrote the article.

www.plantphysiol.org/cgi/doi/10.1104/pp.19.01136

up-regulation of ABA biosynthesis genes, as well as the posttranslational activation of the ABA-deconjugating enzyme BGlu18. Similarly, high levels of allantoin prevent damage caused by salt stress (Irani and Todd, 2016; Lescano et al., 2016; Irani and Todd, 2018). Interestingly, allantoin translocation from roots to shoots is necessary for plant protection. However, how this metabolite is exported from root cells remains unclear.

Allantoin is generated via the biosynthesis of purines and their subsequent oxidative degradation. Xanthine is the first common intermediate for degradation of all purine bases (Zrenner et al., 2006). In the cytosol, xanthine dehydrogenase converts xanthine to uric acid (Hesberg et al., 2004; Werner and Witte, 2011), which is imported into peroxisomes and oxidized by urate oxidase to hydroxyisourate and subsequently converted to allantoin by allantoin synthase (Lamberto et al., 2010). Allantoin is hydrolyzed to allantoic acid through allantoinase (AtALN), which has been localized in the endoplasmic reticulum (ER; Werner et al., 2013). Subsequent catabolic steps occur in this compartment and result in the complete decomposition of the purine ring, releasing carbon dioxide, glyoxylate, and four ammonium ions (Serventi et al., 2010; Werner et al., 2010; Werner et al., 2013). Thus, allantoin transport to the ER can potentially be a necessary event for its degradation, stress signaling, and cell export because (1) the unique enzyme responsible for its catabolism resides in the ER and is strongly down-regulated under stress conditions (Lescano et al., 2016); (2) the ABA-deconjugating enzyme BGlu18 is localized in the ER (Lee et al., 2006), indicating that its physical association with allantoin required for stress signaling occurs in this compartment; and (3) entering the membranous system of the cell, allantoin may be exported through the secretory pathway. However, the subcellular distribution of allantoin and the putative transport systems between cell compartments remain unidentified.

A family of transmembrane proteins able to transport allantoin has been identified in Arabidopsis (*Arabidopsis thaliana*; AtUPS1 to AtUPS5; Desimone et al., 2002). Hydrophobicity analysis of these sequences predicts 10 putative transmembrane domains (TMDs) conserved in all members, with the C- and N termini protruding into the extracellular space. A large cytosolic domain is predicted between transmembrane helices 5 and 6. AtUPS1 and AtUPS2 have been shown to mediate the transport of purine degradation products and pyrimidines when expressed in yeast or *Xenopus* oocytes (Schmidt et al., 2004). Both proteins have high affinities for uracil and its toxic analog 5-fluorouracil (5-FU).

Differently from other family members, AtUPS5 transported allantoin with high affinity and did not use pyrimidines as substrates. AtUPS5 is expressed in cortical cells and endodermis of roots, suggesting that this permease could be involved in long distance transport of allantoin from roots to shoots (Schmidt et al., 2006). It has recently been observed that Arabidopsis mutants in AtUPS5 (*ups5*) were defective in the use of externally supplied allantoin as a sole nitrogen source, indicating that AtUPS5 is necessary for allantoin long distance transport in vivo (Lescano et al., 2016). Moreover, *ups5* mutants were sensitive to salt stress, suggesting that allantoin transport is a critical event for plant protection.

Two alternative splice variants of AtUPS5 were identified by Schmidt et al. (2006). While the longer protein AtUPS5L is predicted to have 10 TMDs, the shorter isoform AtUPS5S would lack two TMDs as the structural consequence of an additional splice event. Alternative splicing modulates gene expression and eventually produces proteins with different functions and/or subcellular localizations (Stamm et al., 2005). While AtUPS5L functions as a cell importer of allantoin, AtUPS5S could not be shown to mediate uptake of allantoin or other purine degradation products when expressed in yeast, suggesting a different transport activity or subcellular localization (Schmidt et al., 2006). However, information about the subcellular fate of AtUPS proteins is scarce. Among the five members of the AtUPS family, only the subcellular localization of AtUPS1 was characterized when expressed in yeast cells. Tagging AtUPS1 with c-myc, either at the N terminus and C terminus, led to ER retention of most of the protein, consistent with folding problems. A similar situation was observed tagging the transporter at the C terminus with GFP (Froissard et al., 2006). On the contrary, the insertion of a small myc-tag inside the central loop of AtUPS1 between predicted transmembrane helices 5 and 6 of AtUPS1 produced functional proteins that reached the plasma membrane of yeast cells.

In this work, AtUPS1, AtUPS5L, and UPS5S tagged in their central loops were localized in distinct plant cell membranes, indicating that they may have different functions. AtUPS1 was detected in the plasma membrane, AtUPS5S in the ER, and AtUPS5L in the plasma membrane, ER, trans-Golgi network/early endosome (TGN/EE), and conspicuously in the cell plate of dividing cells. These data together with studies on the phenotype of knockout and knockdown mutant lines (*ups5*) presented here and previously support the conclusion that both AtUPS5 splice variants play important roles in the connection of ureide metabolism between events occurring in the cytosol and in compartments delimited by the endomembrane cell system. The complementary function of these transporters could possibly contribute to a better understanding of how allantoin is degraded and/or conditionally exported from the roots via the cellular secretory pathway.

RESULTS

Subcellular Localization and Function of AtUPS1 Are Not Affected by the Fusion of eGFP into its Central Loop

To study the subcellular localization of AtUPS in a reliable manner, a molecular tool was first developed in yeast (*Saccharomyces cerevisiae)* using AtUPS1 as a model. The translational introduction of a c-myc sequence in a hydrophilic central loop between the

predicted transmembrane helices 5 and 6 of AtUPS1 produced proteins, which reached the plasma membrane of yeast cells and were able to transport the same substrate range as the native permease. This finding encouraged us to evaluate if the translational fusion of enhanced GFP4 (eGFP4) into the central loop of AtUPS1 (UPS1-eGFP4) would affect its subcellular localization and/or transport activity. The eGFP4 sequence was inserted between Met 183 and Glu 184 of AtUPS1. When expressed in yeast, this fusion protein was able to complement the transport deficiency of *fur4* mutants (Supplemental Fig. S1), indicating that insertion of eGFP4 did not affect the transport function of AtUPS1 at the plasma membrane of yeast cells.

Consecutively, UPS1-eGFP4 was expressed in Arabidopsis plants (Col-0) under the control of the *UBQ10* (*UBIQUITIN10*) promoter. Four independent homozygous lines with a single T-DNA insertion were selected for further studies. All lines showed AtUPS1 localized mainly at the plasma membrane of the root cells, but a weaker intracellular signal surrounding ER was observed (Fig. 1A). After 5-min incubation with the endocytic tracer FM4-64, 84.17 ± 6.34% of UPS1-eGFP4 signal colocalized with FM4-64 signal at the plasma membrane (r = 0.59 ± 0.09; Fig. 1B). These results indicate that UPS1-eGFP4 is present at the plasma membrane, but not in endosomal compartments. A similar subcellular localization of AtUPS1 was previously reported by experiments of heterologous expression in yeast (Froissard et al., 2006).

AtUPS1 showed high transport affinity for uracil and derivatives in yeast, suggesting that it serves as a uracil transporter in planta (Schmidt et al., 2004). Previously characterized transgenic lines with reduced *UPS1* transcript levels (*UPS1* PTGS) were resistant to uracil toxic analog 5-FU. To determine whether constitutive expression of UPS1-eGFP4 increases sensitivity to 5-FU, the growth of wild type, pUBI10:UPS1-eGFP4/wild type, and *UPS1* PTGS plants in Murashige and Skoog (MS) media containing the toxic analog were compared. All lines were affected by 5-FU compared with control conditions (Fig. 1C). Interestingly, pUBI10:UPS1-eGFP4/wild-type plants showed a severe growth retardation compared to wild-type plants. Indeed, wild-type plants showed a reduction of 66% in root length compared with controls, whereas UPS1-eGFP4/wild-type lines presented a reduction of 78% (Fig. 1C). As was previously shown by Schmidt et al. (2004), UPS1 PTGS lines were less affected by 5-FU. These results suggest that UPS1 tagged with GFP in its central loop mediates the uptake of 5-FU into the plant cells. The analysis of the subcellular localization and transport activity of UPS1-eGFP4 in planta suggests that insertion of eGFP into the central loop of AtUPS1 does not affect both subcellular fate and transport function of the protein. This strategy was thus used for further analysis of the subcellular localization of AtUPS5 proteins.

AtUPS5L and AtUPS5S Share the Same Membrane Protein Topology

Two alternative splicing variants of *AtUPS5* transcripts, *AtUPS5L* and *AtUPS5S*, were previously identified, and their putative translational products functionally characterized by heterologous expression in yeast (Schmidt et al., 2006). Membrane protein topology provides crucial information for determining the substrate transport direction between subcellular compartments. The consensus prediction based on 18 different

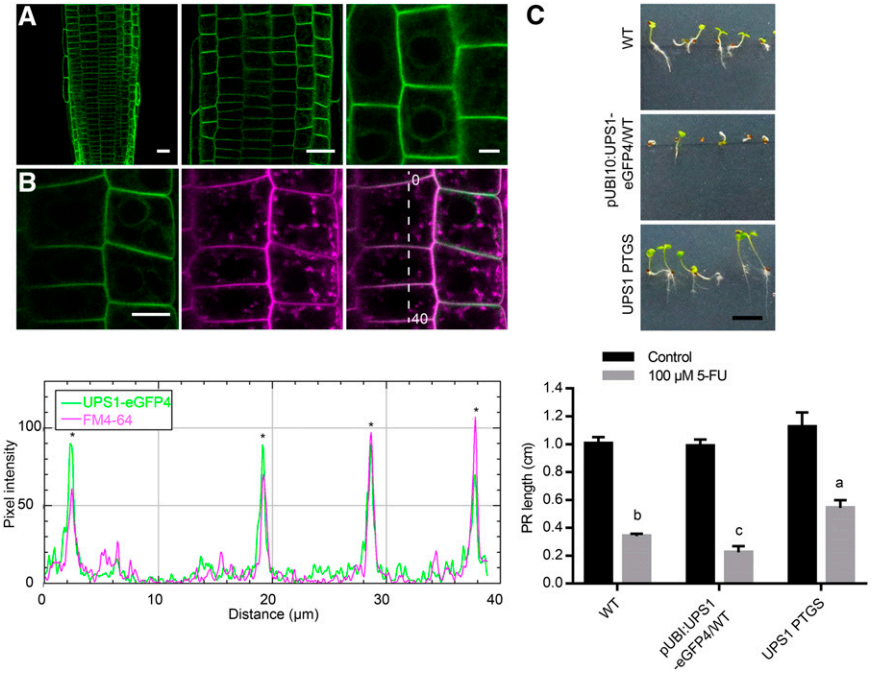

Figure 1. Subcellular localization of UPS1-eGFP4 in Arabidopsis. A, Representative CLSM (confocal laser scanning microscopy) images of roots of 7-d-old Arabidopsis roots expressing pUBI10:UPS1-eGFP4. Scale bars = 20 μm (left, center) and 5 μm (right). B, Colocalization with the endocytic tracer FM4-64. Images taken in the GFP channel (left), FM-64 channel (center), and merged (right) are shown. Scale bars = 10 μm. Intensity profiles for each channel obtained from pixels are marked with the dashed line in (B). The asterisks indicate peaks where signals of both channels overlap. C, Phenotype of wild type (WT), pUBI10:UPS1-eGFP4/wild type, and UPS1 PTGS lines in response to 5-FU. Seedlings were grown on 0.5× MS agar plates without (control) or with 100 μM 5-FU. Photographs were taken after 7 d of grow. Scale bar = 1 cm. The bar graph represents the primary root (PR) lengths of each genotype (mean ± SE, n = 8). Letters indicates significant differences between genotypes ($P < 0.05$, DGC's multiple comparison test).

informatics tools for protein topology determination indicated that both proteins have noncytosolic N- and C terminus, 8 (AtUPS5S) or 10 (AtUPS5L) TMDs, and a large loop protruding into the cytosol (Schwacke et al., 2003).

To gain experimental evidence supporting these predictions, the topology of both proteins was studied using a redox-sensitive GFP (roGFP2; Schwarzländer et al., 2008; Brach et al., 2009). At more negative EGSH (glutathione redox potential), as found in the cytosol, excitation at 488 nm is more efficient, whereas 405 nm is more efficient in exciting roGFP2 in an environment with less negative EGSH, such as the ER lumen (Meyer et al., 2007; Brach et al., 2009). The roGFP2 sequence was translationally fused in the hydrophilic loop of AtUPS5L or AtUPS5S and expressed under the control of the UBIQ10 promoter in wild-type plants. As predicted, both UPS5L-roGFP2 and UPS5S-roGFP2 showed low 405/488 nm fluorescence ratios, indicating a reducing environment close to that measured for the cytosolic control (Fig. 2, A and B). It was concluded that both proteins share the same topology with the loop protruding into the cytosol (Fig. 2C).

AtUPS5 Isoforms Have Different Subcellular Localizations

Alternative splicing often yields proteins that differ in their subcellular distribution. To determine the subcellular localization of the longer isoform AtUPS5L, eGFP4 was inserted between Pro 194 and Glu 195 of the hydrophilic loop. To perform coexpression experiments, we chose the fusion of monomeric red fluorescent protein (mRFP) between Pro 159 and Glu 160 of the central loop of the shorter isoform AtUPS5S. Both proteins were separately expressed under the control of the *UBIQ10* promoter in previously characterized knockout *ups5-1* plants (Lescano et al., 2016). Transcripts of expected sizes were detected in the UPS5L-eGFP4 and UPS5S-mRFP plants by end point reverse transcription–PCR (RT-PCR) using specific primers for each *AtUPS5* splice variant (Supplemental Fig. S2; Schmidt et al., 2006). Full-length complementary DNAs (cDNAs) of UPS5-eGFP4 plants were amplified with specific primers for *UPS5L*, but not with primers for *UPS5S*, indicating that *UPS5L-eGFP4* does not splice as the native, intron-containing transcripts (Supplemental Fig. S2B).

Plants expressing UPS5L-eGFP4 or UPS5S-mRFP showed fluorescence in intracellular compartments surrounding vacuoles of root cells (Fig. 3, A and E). The fluorescent pattern of both UPS5L-eGFP4 and UPS5S-mRFP presented the typical reticular shape of the plant ER (Fig. 3, B and F). Staining of UPS5L-eGFP4 or UPS5S-mRFP roots with ER tracker red or green dyes, respectively, confirmed the ER localization of both UPS5 tagged proteins (Supplemental Fig. S3). Consistently, transient expression of UPS5L-roGFP2 or UPS5S-roGFP2 in *Nicotiana benthamiana* leaves highlighted the typical ER network pattern in the epidermal cells (Supplemental Fig. S4). To perform colocalization experiments of both variants, we crossed pUBI10:UPS5L-eGFP4/*ups5-1* and pUBI10:UPS5S-mRFP/*ups5-1* plants. The resulting offspring showed the same subcellular localization of tagged-UPS5 isoforms that in the parent plants (Fig. 3, G and H). The intracellular GFP signal colocalized 83.98 ± 8.74% with mRFP signal ($r = 0.52 \pm 0.13$) in these plants (Fig. 3I).

UPS5L-eGFP4 plants additionally showed a punctate mobile pattern of the fluorescent signal, suggesting TGN/EE localization and a weak signal at the plasma membrane (Fig. 3, C and D). This pattern was observed only in the green channel, and the corresponding pixels presented higher intensity values than those of the ER in plants expressing both variants (Fig. 3, I and J; Supplemental Fig. S3). A strong GFP signal was also observed at the cell plate in dividing root cells (Fig. 3, A and D). To confirm cell plate localization we used aniline blue that stains callose deposited on the forming cell plate of dividing cells (Mineyuki and Gunning, 1990). UPS5L-eGFP4 but not UPS5S-mRFP colocalized with aniline blue signal in the cell plate of dividing root cells (Fig. 4A; Supplemental Fig. S5).

The subcellular localization of UPS5L in the endocytic pathway was studied in more detail by incubating UPS5L-eGFP4 plants with the endocytic tracer FM4-64. After 20 min of treatment the intracellular UPS5L-eGFP4 signal colocalized 74.17 ± 9.8% ($r = 0.48 \pm 0.09$) with FM4-64 in the root cells (Fig. 4B), indicating that UPS5L-eGFP4 also localized in the endosomal compartments. To identify the fate of UPS5L-eGFP4 in the endosomal pathway, we treated UPS5L-eGFP4 plants with the vesicle traffic inhibitor brefeldin A (BFA). The punctuate signals of UPS5L-eGFP4 and FM4-64 aggregated together in BFA bodies after this treatment (Fig. 4C).

Since specific trans-Golgi markers are found in BFA compartments, we performed colocalization experiments with the vacuolar H^+-ATPase subunit 1 (VHAa-1) that specifically localizes in the TGN/EE (Dettmer et al., 2006). Transgenic seedlings coexpressing UPS5L-eGFP4 and VHA-a1-mRFP showed overlapping punctate patterns (Fig. 4D), indicating that both proteins colocalize in the TGN/EE. Furthermore, image quantification revealed that 72.98 ± 13.21% of the signal overlapped between the green and the red channels ($r = 0.59 \pm 0.05$). Colocalization experiments of UPS5S with FM4-64 and VHA-a1-eGFP indicated that UPS5S is not present in the TGN/EE (Supplemental Fig. S6). In summary, our data indicate that both splice variants of AtUPS5 localize in the ER membranes, but UPS5L is additionally localized in the TGN/EE, in the cell plate of dividing cells and in the plasma membrane.

Allantoin Use Efficiency and Salt-Stress Tolerance Are Fully Rescued in ups5-1 by UPS5L-eGFP4, But only Partially by UPS5S-mRFP Expression

To determine whether UPS5L-eGFP4 and UPS5S-mRFP are able to function as the native isoforms of

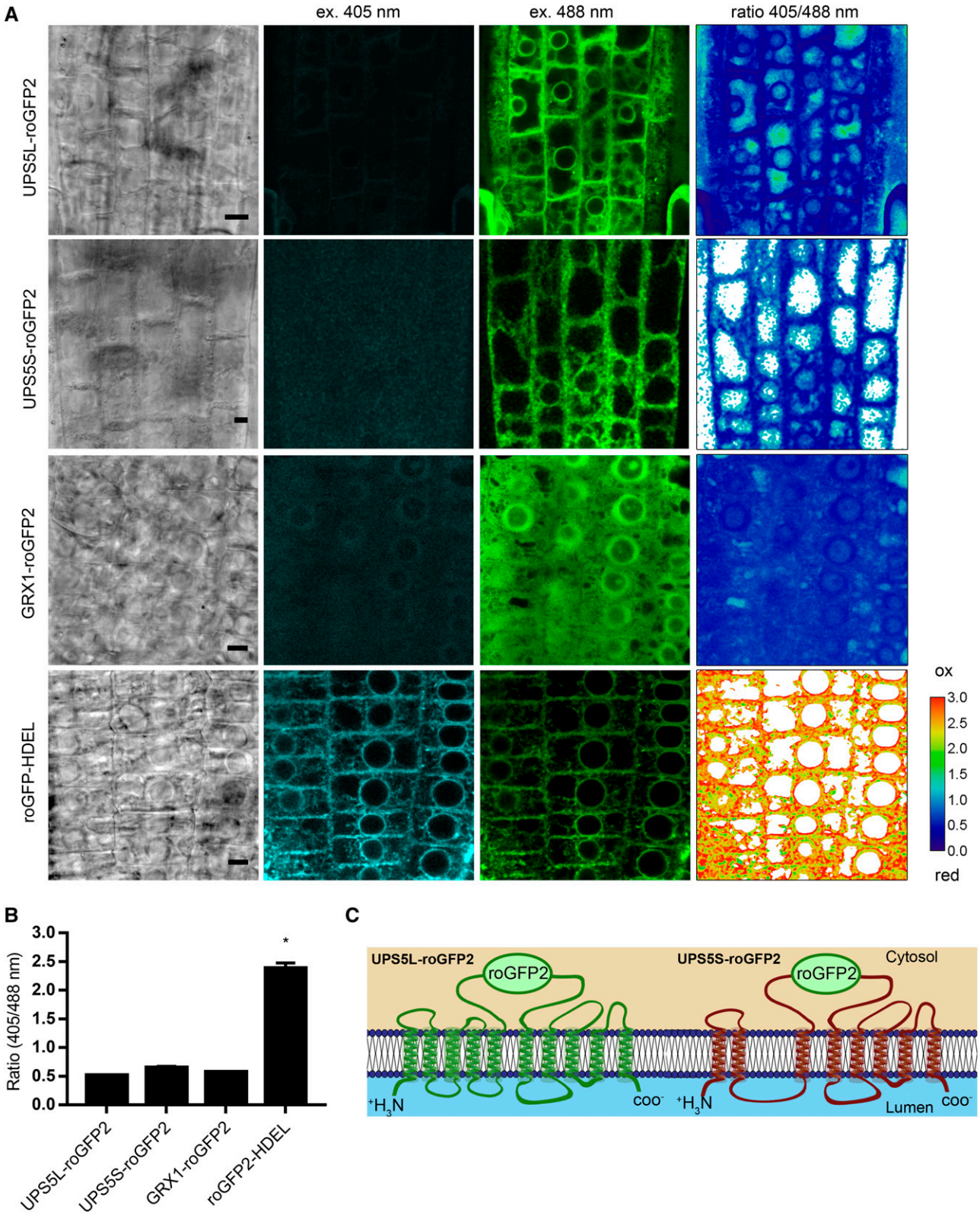

Figure 2. Ratiometric analysis of UPS5L-roGFP2 and UPS5S-roGFP2 expressed in Arabidopsis plants. roGFP2 was inserted into the central loop of UPS5L or UPS5S and expressed in Arabidopsis plants. Roots of 10-d-old-plants were imaged at 405 and 488 nm to detect oxidized and reduced forms of roGFP, respectively. A, Representative CLSM images for pGGZUBI10:UPS5L-roGFP2/wild type or pGGZUBI10:UPS5L-roGFP2/wild type plants, in which roGFP fluorescence was excited (excitation

AtUPS5, transgenic lines expressing these fusion proteins in the genetic background of *ups5-1* and wild-type plants were comparatively studied in nutritional and salt stress experiments. In a first approach, we tested whether transgenic plants expressing UPS5L-eGFP4 or UPS5S-mRFP could use external supplied allantoin as their sole nitrogen source. No phenotypic differences could be observed under control conditions in 0.5× MS medium containing inorganic nitrogen sources (Fig. 5). As previously reported (Lescano et al., 2016), the growth performance of *ups5-1* was significantly decreased in comparison with wild-type plants when allantoin was used as the sole nitrogen source (Fig. 5). When UPS5L-eGFP4 was expressed in the *ups5-1* background, plant growth was restored showing fresh weight and PR length values similar to wild-type plants (Fig. 5, B and C). UPS5S-mRFP/*ups5-1* plants showed 1.3-fold increased biomass compared with *ups5-1* mutants, but did not reach wild-type values (Fig. 5B). In addition, UPS5S-mRFP/*ups5-1* PR length was significantly lower compared with wild type, and no significant differences in PR length were detected between UPS5S-mRFP/*ups5-1* and *ups5-1* plants (Fig. 5C). Similar results were obtained using independent transgenic lines for each splicing variant (Supplemental Fig. S7). Interestingly, root growth performance of *ups5-1* and UPS5S-mRFP/*ups5-1* individual seedlings showed high heterogeneity compared with wild type and UPS5L-eGFP4/ups5-1 plants with allantoin as the sole N source (Fig. 5A). To test if this phenomenon was a result of different germination capacities, we compared the germination rate of wild type, *ups5-1*, UPS5L-eGFP4/*ups5-1*, and UPS5S-mRFP/*ups5-1* in media with inorganic N or allantoin as a sole N source. No significant differences in germination percentage between the genotypes were detected 72 h after exposing the seeds to the light, although slight differences in the germination rate were observed (Supplemental Fig. S8). These data suggest that the expression of UPS5L, but not of UPS5S, is necessary for later developmental events of seedling roots. Moreover, coexpression of both UPS5L-eGFP4 and UPS5S-mRFP in the *ups5-1* background did not alter the phenotype compared with UPS5L-eGFP4/*ups5-1* plants (Fig. 5).

These results suggested that UPS5 proteins have different transport capacities. We analyzed the capability of these plants to restore allantoin translocation from roots to the shoots by transplanting 7-d-old seedlings to media containing 5 mM allantoin for 3 h. No differences in allantoin concentration were detected between genotypes before transplanting (Supplemental Fig. S9). As expected, allantoin content was 65.37% lower in *ups5-1* compared to wild-type shoots 3 h after transplanting. Remarkably, allantoin concentration of UPS5L-eGFP4/*ups5-1* and UPS5S-mRFP/*ups5-1* shoots increased 4.43- and 4.25-fold with respect to *ups5-1* shoots. However, no significant differences in the shoot allantoin content were detected between UPS5L-eGFP4/*ups5-1* and UPS5S-mRFP/*ups5-1* plants. These results demonstrate that both UPS5 proteins are capable of allantoin uptake and transport from roots to shoots, but only UP5L-eGFP4 expression fully restored the capability of allantoin usage as a nitrogen source.

As previously shown, allantoin transport by AtUPS5 confers salt stress tolerance to Arabidopsis plants (Lescano et al., 2016). To determine if the expression of splicing variants fused to fluorescent proteins rescue the response to salt stress in *ups5-1* mutants, 14-d-old wild type, *ups5-1*, UPS5L-eGFP4/*ups5-1*, and UPS5S-mRFP/*ups5-1* plants were transferred to medium without or with 150 mM NaCl for 7 d. *ups5-1* plants were severely damaged by salt as shown by its reduced growth and chlorophyll content with respect to wild-type plants (Fig. 6). On the contrary, UPS5L-eGFP4/*ups5-1* and UPS5S-mRFP/*ups5-1* showed better growth and higher chlorophyll concentrations compared with the *ups5-1* background under salt stress. Furthermore, no significant differences in both fresh weight and chlorophyll content were observed between UPS5L-eGFP4, UPS5S-mRFP, and wild-type plants (Fig. 6). Similar results were obtained by growing these genotypes for 4 d in 0.5× MS containing 100 mM NaCl (Supplemental Fig. S4). Moreover, independent transgenic lines expressing UPS5L-eGFP4 or UPSs-mRFP showed better growth performance compared with the *ups5-1* background (Supplemental Fig. S10). Taken together, these results revealed that transformation of the *ups5-1* mutant with UPS5L-eGFP4 or UPS5S-mRFP fusions restored its ability to tolerate salt stress to that of the wild type, thus demonstrating that the fusion proteins are functional.

AtUPS5L Regulates Long Distance Transport of Allantoin under Salt Stress

The complementation of *ups5-1* mutants by the constitutive expression of UPS5L or UPS5S in Arabidopsis suggests that both variants are capable of allantoin transport for salt stress tolerance (Fig. 6; Supplemental

Figure 2. (*Continued.*)
wavelenght [ex.]) at 405 and 488 nm, and the corresponding ratio images (405 nm/488 nm). The ratio images were illustrated using the "Thermal" LUT setting pixel values between 0 (reduced) and 3 (oxidized). At least three independent lines for each construct were analyzed. Plants expressing free cytosolic (GRX1-roGFP2) or ER (roGFP2-HDEL) roGFP2 were used as controls (Meyer et al., 2007; Brach et al., 2009). Scale bars = 5 μm. B, Fluorescence ratios for UPS5L-roGFP2, UPS5S-roGFP2, and controls. The bar graph represents values measured from regions of interest of the ratio images (mean ± SE, $n = 7$). Asterisks indicates significant differences in comparison with GRX1-roGFP2 plants ($P < 0.05$, Kruskal-Wallis multiple comparison test followed by Dunn's test). C, Schematic representation of the topology of AtUPS5 isoforms fused to roGFP2 used in this experiment.

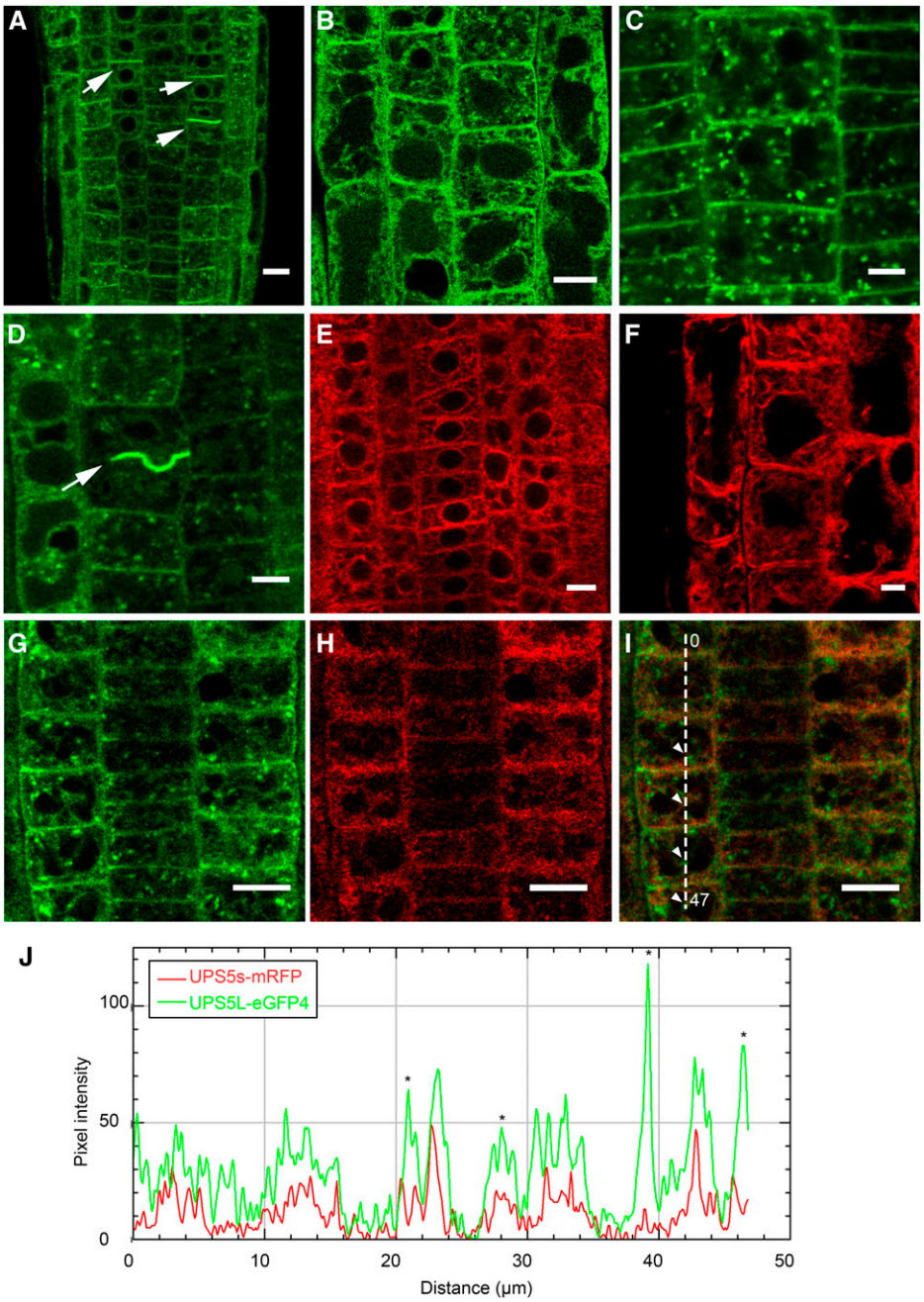

Figure 3. Subcellular localization of AtUPS5L and AtUPS5S in Arabidopsis roots. A to D, Representative CLSM images of 7-d-old Arabidopsis roots expressing pUBI10:UPS5L-eGFP4. Details of the GFP signal in the ER, vesicles, and cell plate are shown in (B), (C), and (D), respectively. Arrows in (A) and (D) indicate the distribution of UPS5L-eGFP4 in the cell plates of dividing cells. E and F, Representative CLSM images of 7-d-old Arabidopsis roots expressing pUBI10:UPS5S-mRFP. Details of the mRFP signal in the ER are shown in (F). G to I, Representative CLSM images of 7-d-old Arabidopsis roots coexpressing pUBI10:UPS5L-eGFP4 and pUBI10:UPS5S-mRFP. Images taken in the GFP channel (G), RFP channel (H), and merged (I) are shown. Scale bars = 10 μm (A, B, G, H, I), 5 μm (C, D, F), and 20 μm (E). J, Intensity profiles for each channel obtained from pixels marked with the dashed line in (I). The asterisks designate peaks that correspond to the points indicated with white arrows in (I).

Figs. S9 and S11). However, the relative levels of the native splicing variants could be differentially modulated under salt stress. The mRNA levels of *AtUPS5* splicing variants were assessed using RT-quantitative PCR (RT-qPCR) analysis of Arabidopsis plants subjected for 24 h to salt stress or control conditions. No significant differences were detected in *AtUPS5L* or *AtUPS5S* expression in the shoots of plants treated with NaCl compared with controls (Fig. 7A). In contrast, salt treatment increased *AtUPS5L*, but not *AtUPS5S* transcript levels in the roots. Indeed, salt stress conditions enhanced *AtUPS5L* mRNA levels in the roots compared with shoots, whereas no statistically significant changes in *AtUPS5S* root-to-shoot expression were found (Fig. 7B). This result suggest that *AtUPS5L* expression is specifically up-regulated under salt stress.

This observation led us to study the potential role of the native AtUPS5 in allantoin transport during salt stress. Wild-type and *ups5-1* plants grown in 0.5× MS with 5 mM allantoin for 2 weeks were transferred to medium without or with 150 mM NaCl. In general, allantoin content increased in shoots of plants that were grown with allantoin compared with those grown without allantoin (Supplemental Fig. S12A). Remarkably, the allantoin content in the shoots was higher in plants grown under salt stress. However, *ups5-1* plants

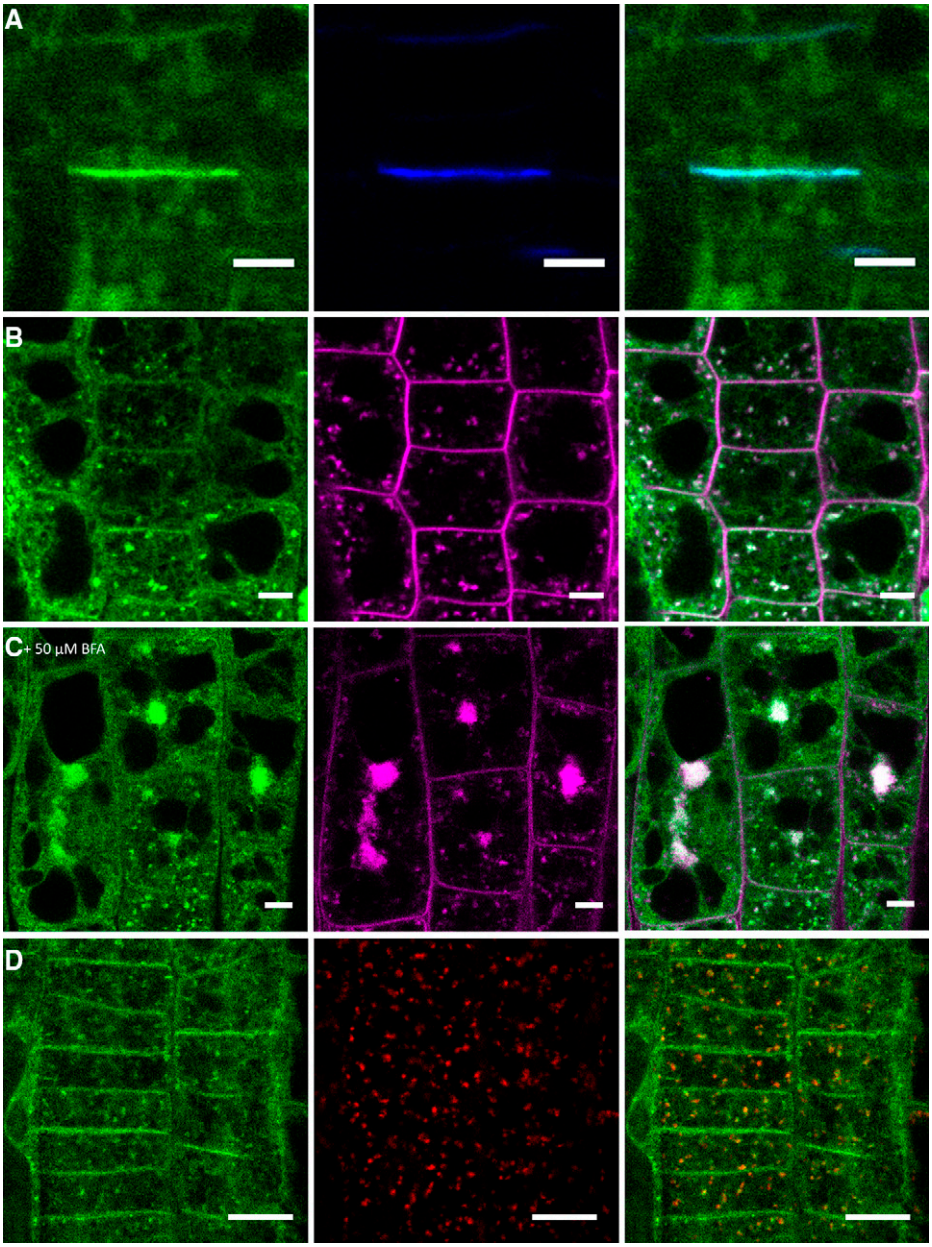

Figure 4. Localization of UPS5L:eGFP4 in the cell plate and in the TGN/EE. A, Representative CLSM images of 7-d-old Arabidopsis roots expressing pUBI10:UPS5L-eGFP4 treated with 0.01% (w/v) aniline blue for 15 min. Aniline blue stains callose deposited on the forming cell plate. Images taken in the GFP channel (left), Aniline blue channel (center), and merged (right) are shown. B and C, Representative CLSM images of 7-d-old Arabidopsis roots expressing pUBI10:UPS5L-eGFP4 treated with 1 μM FM4-64 for 20 min. Images taken in the GFP channel (left), FM4-64 channel (center), and merged (right) are shown. Images were taken before (A) or after (B) 1 h of 50 μM BFA incubation. D, Representative CLSM images of 7-d-old Arabidopsis roots coexpressing pUBI10:UPS5L-eGFP4 and VHAa-1-mRFP. Images taken in the GFP channel (left), RFP channel (center), and merged (right) are shown. Scale bars = 5 μm.

showed lower levels of allantoin in the shoots, whereas allantoin content in the roots was ~3-fold higher in *ups5-1* than in wild-type plants (Supplemental Fig. S12, A and B). Therefore, the root-to-shoot allantoin content ratio clearly decreased in wild-type plants, but increased in *ups5-1* mutants (Supplemental Fig. S12C). Interestingly, wild-type plants could alleviate chlorophyll loss when previously grown with allantoin, showing a chlorophyll concentration similar to the control experiment (Supplemental Fig. S12D). By contrast, *ups5-1* mutants failed to restore chlorophyll content after salt stress even when previously grown with allantoin. These results suggest that native AtUPS5 mediates allantoin transport required for salt stress tolerance. Moreover, the specific induction of *AtUPS5L* expression by salt indicates that this isoform has a predominant role in mediating allantoin transport under salt stress in Arabidopsis.

DISCUSSION

The assessment of transporter subcellular fate is crucial to understand its molecular function. Since prediction tools for membrane protein topology indicate that both ends of UPSs protrude into non-cytoplasmic compartments, which can potentially cause folding and/or sorting defects (Froissard et al., 2006), fluorescent proteins were introduced in a hydrophilic loop predicted to reside in the cytosol (Schwacke et al., 2003). The amino acid sequence of this domain is evolutionary nonconserved in the UPS

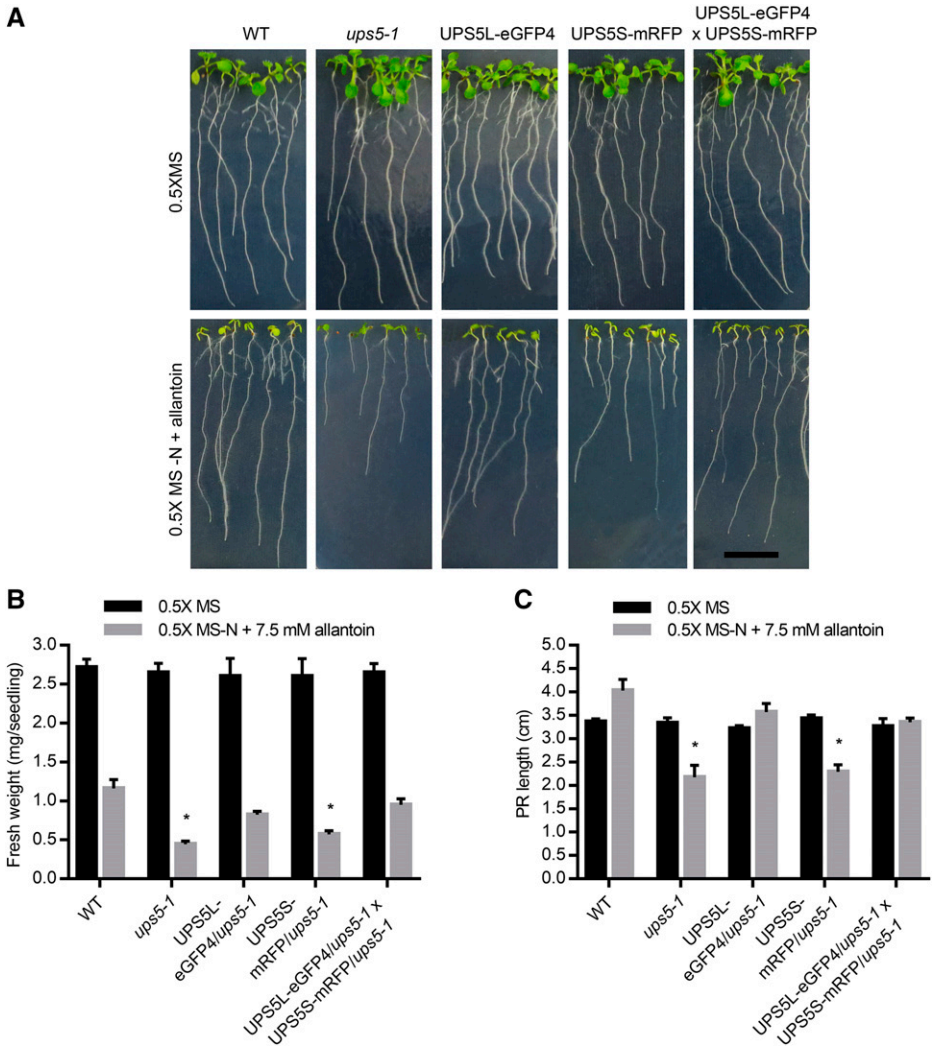

Figure 5. Phenotype of UPS5L-eGFP4, UPS5S-mRFP, and UPS5L-eGFP4 × UPS5S-mRFP/ups5-1 plants grown with allantoin as a nitrogen source. Wild type (WT), *ups5-1*, UPS5L-eGFP4/*ups5-1*, UPS5S-mRFP/*ups5-1*, and UPS5L-eGFP4 x UPS5S-mRFP/*ups5-1* plants were grown in either solid 0.5× MS standard medium containing 30 mM total inorganic nitrogen (control) or 0.5× MS medium without nitrogen supplemented with 7.5 mM allantoin as a sole nitrogen source for 7 d. A, Representative seedlings grown on vertical plates. Scale bar = 1 cm. The bar graphs represent the fresh weights (B) or PR lengths of each genotype (C; mean ± SE, $n = 5$ for [B] or = 8 for [C], respectively). Asterisks indicates significant differences between genotypes and the wild type ($P < 0.05$, Kruskal-Wallis multiple comparison test followed by Dunn's test). Similar results were obtained using two independent lines of UPS5L-eGFP4/*ups5-1* and UPS5S-mRFP/*ups5-1* (Supplemental Fig. S7).

family, suggesting that it may structurally serve as a spacer between TMDs. This strategy has not been frequently used to study plant membrane proteins. Nevertheless, some examples illustrate its relevance particularly to understand localization of intracellular membrane proteins (Simon et al., 2016).

The resulting proteins, UPS1-eGFP4, UPS5L-eGFP4, and UPS5S-mRFP, were in all cases functional when expressed in Arabidopsis plants (Figs. 1C, 5, and 6; Supplemental Figs. S9–S11). Each fusion protein showed a different localization pattern in cell membranes suggesting that the fluorescent protein did not per se affect protein trafficking. UPS1-eGFP4 localized at the plasma membrane (Fig. 1, A and B). This finding is consistent with the localization observed previously in yeast cells and suggests that UPS1 acts as a cell importer in vivo (Froissard et al., 2006). Supporting this notion, expression of UPS1-eGFP4 under the control of a constitutive promoter enhanced plant susceptibility to 5-FU (Fig. 1C). Conversely, these plants did not improve their growth performance if allantoin was used as a sole nitrogen source. This may reflect the lower affinity of UPS1 for allantoin with respect to pyrimidine substrates and/or that the presence of other UPS(s) in wild-type plants may be sufficient to fulfill allantoin uptake function.

Two possible isoforms of AtUPS5 can be deduced from mRNA splicing variants. While UPS5L is able to import oxidized purines such as xanthine, uric acid, and allantoin, but also uracil into yeast cells, no transport function could be determined for UPS5S (Schmidt et al., 2006). This failure can be explained in several ways including no functionality in yeast, other substrate specificity, or intracellular localization. In this work, it could be shown that UPS5S-mRFP localizes to the ER of plant cells (Fig. 3, E and F; Supplemental Figs. S3 and S4). Moreover, UPS5S-mRFP was able to partially complement allantoin transport deficiency observed in *ups5* mutants (Figs. 5 and 6; Supplemental Figs. S9–S11). This indicates not only that the fusion protein is functional, but also demonstrates for the first time that UPS5S is involved in allantoin transport through intracellular membranes. UPS5L-eGFP4 could be localized in the ER, but also in TGN/EE, plasma

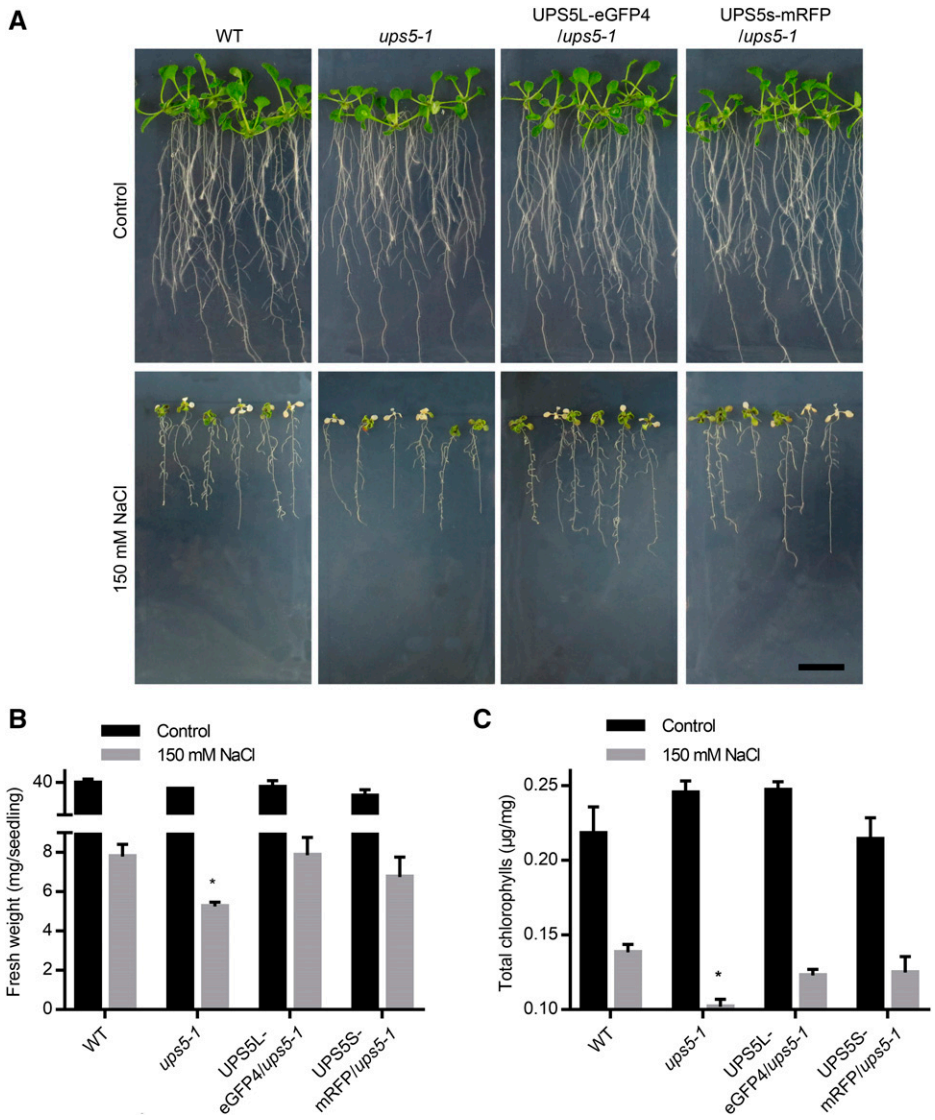

Figure 6. Response of UPS5L-eGFP4 and UPS5S-mRFP lines to salt stress. Fourteen-day-old wild type (WT), *ups5-1*, UPS5L-eGFP4/*ups5-1*, and UPS5S-mRFP/*ups5-1* seedlings were transferred to solid 0.5× MS medium supplemented with 0 (control) or 150 mM NaCl for 7 d. A, Representative seedlings grown on vertical plates. Scale bar = 1 cm. The bar graphs represent the fresh weights (B) or chlorophyll content of each genotype (C; mean ± SE, $n = 4$). Asterisks indicate significant differences between genotypes ($P < 0.05$, DGC 's multiple comparison test). Similar results were obtained using two independent lines of UPS5L-eGFP4/*ups5-1* and UPS5S-mRFP/*ups5-1* (Supplemental Fig. S10).

membrane, and conspicuously in mitotic cell plate membranes (Figs. 3, A and D, and 4A; Supplemental Figs. S3–S5). Expression of UPS5L-eGFP4 in the *ups5-1* genetic background rescued the wild-type phenotype in all conditions tested (Figs. 5 and 6; Supplemental Figs. S9–S11). The independent capacity to complement *ups5* mutants shows that both isoforms have overlapping cell functions. However, some growth restrictions (deficiencies) remained by single UPS5S-mRFP expression indicating nonredundant functions (Fig. 5).

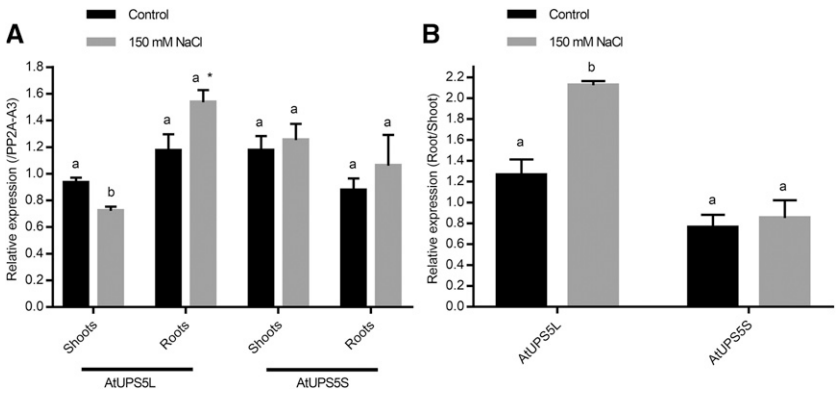

Figure 7. Expression of AtUPS5 splice variants during salt stress. Twenty-one–day-old wild-type plants grown in 0.5× solid MS medium were transferred to solid 0.5× MS medium supplemented with 0 (control) or 150 mM NaCl for 24 h. A and B, Expression of AtUPS5L and AtUPS5S in the shoots and roots. The bar graphs represent the expression level relative to AtPP2A-A3 (A) and root-to-shoot expression (B; mean ± SE, $n = 3$). Asterisks indicates significant differences between roots and shoots, and letters indicates significant differences between treatments ($P < 0.05$, DGC's multiple comparison test). Ct and ΔCt values are shown in Supplemental Table S3.

AtUPS5L structurally resembles the general configuration of plant UPS (Desimone et al., 2002). Thus, it is probable that the AtUPS5S isoform could have evolved to fulfill specialized functions in the ER. Interestingly, all members of the UPS family have highly conserved Ser/Thr residues in the second hydrophilic domain protruding into the cytosol, which are absent in the UPS5S isoform. PIN transporters need to be phosphorylated at Ser/Thr residues localized in an intracellular hydrophilic loop to reach the plasma membrane and to be polarly distributed (Michniewicz et al., 2007). Whether phosphorylation of UPS is a necessary condition to leave the ER remains to be established.

To assign a functional position of each isoform in cellular metabolism requires an understanding of the most probable transport direction under physiological conditions. According to prediction tools, the UPS protein topologies follow a general building plan with 10 TMDs, a central cytoplasmic loop, and noncytoplasmic N and C termini (Fig. 2C). AtUPS5L and other UPS proteins studied so far are able to transport their substrates into the cytosol when expressed in yeast (Desimone et al., 2002; Pélissier et al., 2004; Schmidt et al., 2004; Schmidt et al., 2006; Collier and Tegeder, 2012). Since the domain orientation of AtUPS5S is similarly predicted, but two transmembrane domains are absent and no transport data are available so far, the protein topology in the membrane of AtUPS5S was studied in comparison with AtUPS5L. The experimental evidence presented here indicates that AtUPS5L and AtUPS5S share the same topology and therefore they would transport in the same direction (Fig. 2, A and B). However, at least two additional aspects have to be considered, such us the relative substrate concentrations in the compartments and specially the energization of the transport by proton cotransport demonstrated for AtUPS5L (Schmidt et al., 2006). Allantoin is produced in the peroxisomes from uric acid in the purine degradation pathway, and it reaches the cytosol via an unknown mechanism (Lamberto et al., 2010; Werner et al., 2013). In addition, allantoin can be imported into the cytosol from the extracellular space. On the other hand, the unique gene product for allantoin degradation (allantoinase or AtALN) has been localized in the ER lumen (Werner et al., 2010). These findings predict a higher allantoin concentration in the cytosol than in the ER when allantoinase is expressed. Since AtUPS5L and other UPSs can transport their substrates against a concentration gradient using a H^+ concentration force, the pH at each side of the membrane would regulate the transport direction. Assuming a single H^+ cotransported with each substrate molecule, for example, allantoin, and a pH difference of 2.0–3.0 between apoplast and cytosol, AtUPS5L present at the plasma membrane would be able to transport a substrate molecule 100–1000 times against a concentration gradient in the direction of the cytosol. The pH difference between the lumen of TGN and cytosol in plant cells has been reported to be 1.0–1.5 under nonstress conditions (Shen et al., 2013; Luo et al., 2015). Thus, AtUPS5L in the TGN would transport allantoin 10 times against a concentration gradient into the cytosol. Here, it is important to note that cytosolic acidification can occur under stress conditions especially under salt stress, for example, by the exchange of cytosolic Na^+ by vacuolar H^+ (Kader and Lindberg, 2010). Under stress, the transport velocity of AtUPS5L would be lower or even the transport direction may potentially be inverted. The pH in the cytosol and ER lumen is similar with reported differences between 0.1 and 0.2 (Shen et al., 2013). Therefore, the transport direction by AtUPS5L and AtUPS5S would possibly be more determined by the allantoin concentration than the H^+ concentration. Moreover, there is no experimental evidence indicating that transport by AtUPS5S is H^+ coupled. Some transporter families, for example, plant ENTs, have members transporting their substrates either in a H^+-dependent or independent manner (Wormit et al., 2004).

A comprehensive model illustrated in Figure 8 summarizes the present knowledge on subcellular compartmentalization of allantoin metabolism and the proposed function of AtUPS5L and AtUPS5S in cortical and endodermal cells of roots. In the basal metabolism, allantoin is probably produced only in low amounts as an intermediary metabolite of purine degradation to recycle C and N (Fig. 8A). Allantoin is produced in the peroxisomes, but the degrading enzyme, allantoinase, resides in the ER lumen. Although the mechanism of allantoin leaving peroxisomes is still unknown, the presence of both AtUPS5L and AtUPS5S in the ER can explain how allantoin reaches the ER. In this compartment, allantoinase activity can degrade allantoin for further nutrient recycling. By moderate elevation of allantoin levels or lower allantoinase expression in the cell, AtUPS5L present in the TGN can possibly salvage allantoin molecules to the cytosol avoiding exocytosis through the secretory pathway. In addition, allantoin can be imported into the cells from the environment as a backup compound for N nutrition. AtUPS5L or other AtUPS are candidates that may allow transport across the plasma membrane. The presence of other allantoin transporters in the root is suggested by the detection of allantoin in *ups5-1* shoots (Supplemental Fig. S9). However, higher allantoin levels were detected in plants expressing UPS5. Moreover, the similar transport capacities of UPS5L-eGFP4 and UPS5S-mRFP in planta and their colocalization in the ER membranes suggest that allantoin may enter into the membranous intracellular system by the ER (Fig. 3). Under conditions that promote an important increase of allantoin concentration in root cells, this basal transport system may be able to allow allantoin to pass through the endodermis for long distance transport to the shoot using the water stream in the xylem (Supplemental Figs. S9 and S12, A–C). Figure 8B illustrates this possibility in the particular context of salt stress. Epidermis, cortex, and endodermis cells in direct contact with a saline environment will suffer important metabolic changes. Nucleic

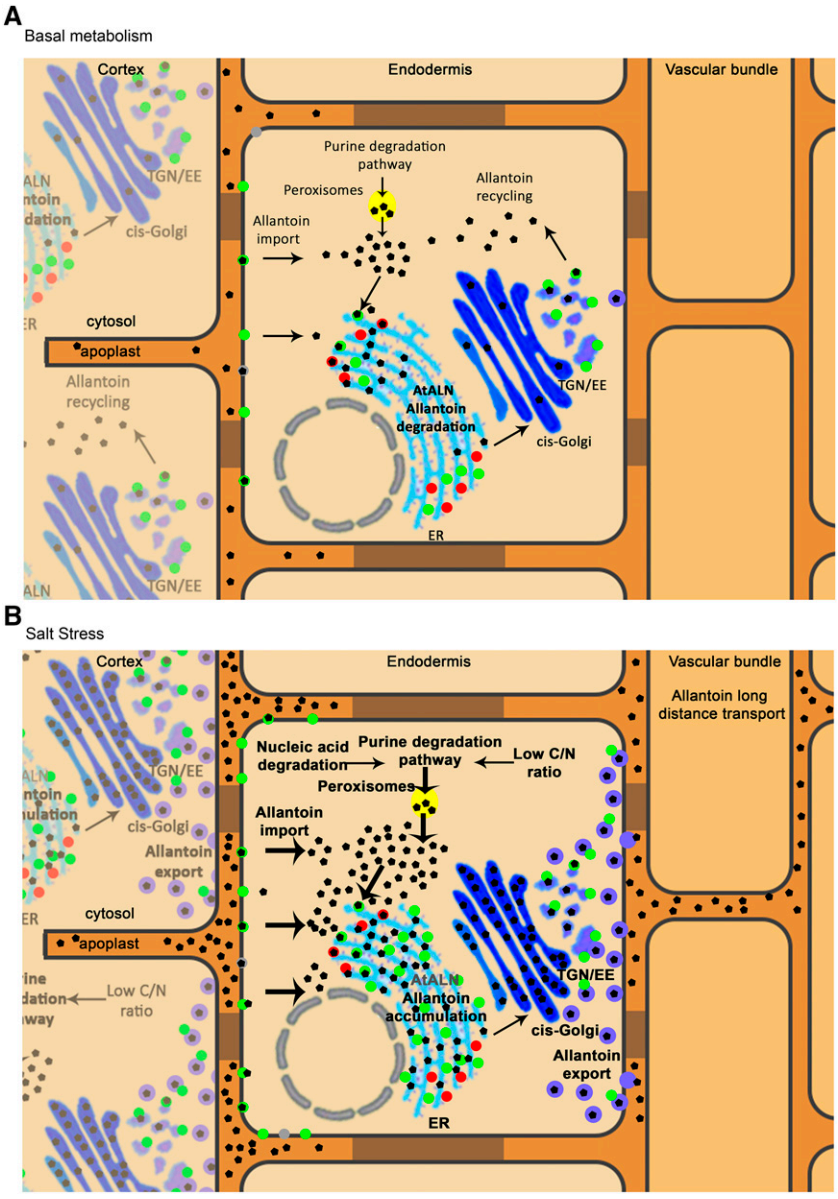

Figure 8. Scheme of allantoin transport between cell compartments and root tissues under basal and stress conditions. The movement of allantoin as well as the distribution of AtUPS proteins in the cell membranes of roots in basal metabolism (A) and salt stress (B) are illustrated. Possible routes of allantoin translocation between root tissues under such conditions are also represented. The position of AtUPS1 (gray circles), AtUPS5L (green circles), and AtUPS5S (red circles) in the secretory pathway is shown. Black pentagons represent the relative amount of allantoin in peroxisomes (yellow), endoplasmic reticulum (light blue), Golgi Apparatus (blue), and TGN/EE (violet), as well as in cytosol (cream) and apoplast (orange). Arrows show possible routes contributing to allantoin increase, representing transport process or metabolic pathways, and thicker arrows symbolize possible increases in the transport activity or metabolism, respectively. Major processes that modulate allantoin distribution between cell compartments and tissues in the plant roots are written in bold letters. The modulation of AtALN (allantoinase) expression under basal and stress conditions is presented.

acid degradation and/or increased purine biosynthesis would activate the purine degradation pathway increasing allantoin concentrations (Brychkova et al., 2008; Irani and Todd, 2016; Lescano et al., 2016; Soltabayeva et al., 2018; Casartelli et al., 2019). Associated with these events, a strong transcriptional down-regulation of allantoinase will occur causing allantoin accumulation in the membranous intracellular system (Irani and Todd, 2016; Lescano et al., 2016). In addition, the cytosol will become more acidic due to mechanisms of Na^+ exclusion via H^+ antiport. This may be important to disable allantoin salvage through AtUPS5L in the TGN. In this way, allantoin accumulated in vesicles may be secreted to the root vascular system. AtUPS5L would be the predominant isoform under salt stress acting in allantoin import to the cytosol and the subsequent transport to the ER (Figs. 7 and 8).

Interestingly, allantoin has been suggested to physically interact with the ABA deconjugating enzyme AtBGlu18, which resides in the ER, suggesting that accumulation of allantoin in the ER would be important to enhance the concentration of the active form of ABA and subsequent stress signaling (Lee et al., 2006; Watanabe et al., 2014). Moreover, allantoin has been found to influence the antioxidant capacity of plants, acting as potential scavengers of ROS (Brychkova et al., 2008) or enhancing the expression or activity of several antioxidant and stress response encoding genes independently of ABA signaling (Irani and Todd, 2018; Nourimand and Todd, 2019). ROS increase in plants subjected to salt stress through mechanisms involving NADP-oxidase in the apoplast and light driven O_2 reduction in chloroplasts (Miller et al., 2010). In this scenario the accumulation of allantoin in vesicles could be

required for its export from the root to the apoplast for ROS scavenging and/or to the vascular system to trigger antioxidant defenses in the shoots (Fig. 8; Supplemental Fig. S12). A similar mechanism would operate under other abiotic stresses in which accumulated allantoin has been suggested to mediate stress response (Watanabe et al., 2014; Irani and Todd, 2016; Nourimand and Todd, 2016).

Similar export systems for allantoin allowing transport to the shoot can be proposed in other physiological contexts. For example, it would be interesting to know if a similar transport mechanism is relevant for allantoin translocation in nodulated tropical legumes.

The transport function of AtUPS5L in cell plate membranes is currently unknown. Interestingly, the shorter PR phenotype of *ups5-1* mutants could be complemented by UPS5L-eGFP4 expression, but not by UPS5S-mRFP, indicating a specific function for AtUPS5L in root growth (Fig. 5). Further experiments should investigate if cell division is affected in *ups5-1* mutant roots.

CONCLUSION

The analysis of AtUPS5L and AtUPS5S subcellular localization presented here provide key information to understand the cell function of these transporters. Our data predict that under nonstress conditions, AtUPS5L and AtUPS5S may be involved in allantoin degradation for nutrient recycling. Under stress, both genes may be necessary for allantoin export via vesicles of the secretory pathway allowing allantoin translocation from roots to shoots, with a predominant role of AtUPS5L.

MATERIALS AND METHODS

DNA-Cloning

DNAs for all constructs were amplified by PCR using Phusion High-Fidelity DNA Polymerase (Thermo Scientific) from genomic DNA or cDNA obtained from wild-type plants. Fragments were cloned into pJet1.2 using CloneJET PCR Cloning Kit (Thermo Scientific) and sequenced (Macrogen). Restriction enzymes and T4 DNA ligase for cloning were supplied by Thermo Scientific. Constructs (Supplemental Table S1) were generated using oligonucleotides listed in Supplemental Table S2 by using standard cloning methods or the GreenGate system (Lampropoulos et al., 2013).

Plant Materials and Growth Conditions

Arabidopsis (*Arabidopsis thaliana*) ecotype Col-0 was used as the wild type. Homozygous seeds of Salk_044810 line (designated *ups5-1*) were previously characterized by Lescano et al. (2016).

For plant growth, seeds were first stratified at 4°C for 3 d. After imbibition, germinating seeds were placed in a growth chamber (day 0 for experimental treatments) under a 16-h light/8-h dark photoperiod at 22°C and a light intensity of 100–150 μmol photons $m^{-2}s^{-1}$ on 0.5× MS plates (1% w/v agar) or on soil:vermiculite (1:1) mix.

Nicotiana benthamiana plants were grown under a 16-h light/8-h dark photoperiod at 24°C and a light intensity of 100–150 μmol photons $m^{-2}s^{-1}$ on soil:vermiculite (1:1) mix.

Plant Transformation and Isolation of Transgenic Lines

pCUBI:UPS1-eGFP4, pCUBI:UPS5L-eGFP4, or pCUBI:UPS5S-mRFP constructs were introduced into *Agrobacterium* strain C58 for transformation of wild-type or *ups5-1* plants. Eight- to 10-week-old Arabidopsis plants were transformed using the floral dip method (Clough and Bent, 1998), and transgenic plants (T1 to T3 generations) were selected using hygromycin B (InvivoGen). Different T2 lines were screened by CLSM, and four independent homozygous lines with a single T-DNA insertion for each construction were selected for further studies. Independent lines of pCUBI10:UPS5L-eGFP4/*ups5-1* and pCUBI10:UPS5S-mRFP/*ups5-1* were crossed for phenotype analysis and colocalization experiments. pCUBI10:UPS5L-eGFP4/*ups5-1* or pCUBI10:UPS5S-mRFP/*ups5-1* plants were crossed with VHAa-1-mRFP or VHAa-1-eGFP, respectively (Dettmer et al., 2006), for colocalization experiments.

For ReTA experiments, pGGZUBI10:UPS5L-roGFP2 or pGGZUBI10:UPS5L-roGFP2 constructs were introduced into *Agrobacterium* strain ASE1 for transformation of 8- to 10-week-old wild-type plants. Transgenic plants (T1 to T2 generations) were selected using BASTA (glufosinate ammonium). Different T2 lines were screened by CLSM, and at least four independent lines with a single T-DNA insertion for each construction were selected for further studies.

For transient expression of UPS5L-roGFP2 or UPS5S-roGFP2, 3- to 4-week-old *N. benthamiana* plants were infiltrated with *Agrobacterium* strain ASE1 transformed with pGGZUBI10:UPS5L-roGFP2 or pGGZUBI10:UPS5L-roGFP2, respectively. Single *Agrobacterium* colonies were grown in 10-mL LB with appropriate antibiotics at 180 RPM at 28°C overnight. After centrifugation at 4500 RPM at 4°C for 15 min, pellets were resuspended in 3-mL infiltration solution (10 mM MES-K(OH) [pH 5.6], 10 mM $MgCl_2$, 150 μM Acetosyringon). The optical density at 600 nm was adjusted to 0.7–0.8 by adding the correct amount of infiltration solution. The solutions of Agrobacteria containing the construct of interest were mixed with Agrobacteria containing silencing inhibitor K19 (1:1) and incubated at room temperature for 2 to 3 h. The lower side of *N. benthamiana* leaves was infiltrated with a 1-mL syringe. The analysis of infiltrated leaves was carried out under the microscope 3 to 4 d after infiltration.

Stress and Nutritional Assays

In all experiments, seeds were sown on 0.5× MS vertical plates and stratified for 3 d at 4°C. Then, plates were placed vertically in a growth chamber under a 16-h light/8-h dark photoperiod at 22°C and a light intensity of 120 μmol photons $m^{-2}s^{-1}$. To test the ability of transgenic lines to use allantoin as a sole nitrogen source, plants were germinated and grown in vertical plates containing 30 mM total nitrogen. Standard 0.5× MS medium (Sigma-Aldrich) or 0.5× MS without nitrogen medium (M531, PhytoTechnology Laboratories) supplemented with 7.5 mM allantoin (Sigma-Aldrich) was used. Germination rate was measured as radicle emergence after exposing the imbibed seeds to the light. After 7 d both fresh weight and root length were measured.

To test the capacity of transgenic lines to translocate allantoin from root to the shoots, plants were germinated and grown for 7 d on 0.5× MS vertical plates. Afterward, plants were transferred to 0.5× MS plates with 5 mM allantoin for 3 h. Material was stored at −20°C for allantoin quantification.

For salt stress experiments, plants were germinated and grown for 14 d on 0.5× MS vertical plates. Afterward, plants were transferred to 0.5× MS vertical plates containing 0 or 150 mM NaCl. Fresh weight per plant was measured after 7 d of transplanting. Additional material was stored for chlorophylls quantification. In a second approach, 4-d-old plants germinated and grown in 0.5× MS vertical plates were transferred to 0.5× vertical plates plus 0 or 100 mM NaCl. After 3 d fresh weight was measured.

For expression experiments, plants were transferred to 0.5× MS vertical plates containing 0 or 150 mM NaCl. Material was frozen and stored at −80°C for RNA extraction and RT-qPCR.

Determination of Root Lengths

Primary root lengths were measured with FIJI (Schindelin et al., 2012).

Determination of Allantoin and Total Chlorophylls

Plant material was dried overnight at 65°C, and the dry weight was measured. Allantoin was obtained by incubation of plant samples in 6.25 mM K_2PO_4/KH_2PO_4 buffer pH 7 for 20 min at 100°C and subsequent centrifugation for 5 min at 14000 RPM. Allantoin present in the supernatants was quantified

using differential analysis of glyoxylate derivatives (Vogels and Van Der Drift, 1970). Chlorophylls were measured from fresh material as described previously (Vernon, 1960).

Expression Analysis

For expression analysis, total RNA from plants was extracted with Tri Reagent according the manufacturer's protocol (Molecular research center). cDNA was synthesized with RevertAid Premium M-MuLV Reverse Transcriptase (Thermo Scientific) and used for PCR reactions. AtUPS5L and AtUPS5S fragments were amplified RT-qPCR using primers previously optimized to identify AtUPS5 splicing variants (Schmidt et al., 2006). For *AtUPS5L* (*AtUPS5S*), primers P19 (P21) and P20 were used to amplify a 238 (208) bp fragment by PCR. A 641-bp fragment of *AcACT2* gene was amplified by PCR using primers P22 and P23, and used as a control (Supplemental Table S2).

For RT-qPCR, total RNA was extracted with RNeasy Plant Mini Kit (Qiagen) according the manufacturer's protocol. cDNA was synthesized with RevertAid Premium M-MuLV Reverse Transcriptase (Thermo Scientific). The reverse transcribed products were amplified with SG qPCR Master Mix (Roboklon) in a 96-well plate Chromo4 Real-Time PCR System (Bio-Rad). Primers were designed with QuantPrime qPCR primer design tool (https://www.quantprime.de/; Supplemental Table S2).

The thermal profile of the RT-qPCR reactions was 95°C for 15 min, 40 cycles of 95°C for 15 s, 60°C for 30 s, and 72°C for 15 s. Moreover, to analyze the quality of the dissociation curves, the following program was added after the 40 PCR cycles: 72°C for 7 min, followed by a constant increase of the temperature from 40°C to 90°C. Ct and Efficiency (E) values were calculated with Opticon Monitor 3.1 software. Relative expression values were calculated using E-ΔCt method (Pfaffl, 2004) using *AtPP2A-A3* (At1g13320) and *AtUBI10* (At4g05310) as housekeeping genes (Supplemental Table S2).

Imaging and Colocalization Experiments

Laser scanning confocal microscopy was performed using a Leica TCS SP5II with an HCX PL APO lambda blue 63.0 × 1.20 water UV lens or with Olympus FV1200 laser scanning microscope with a 60× silicone-immersion objective lens. The following excitation and detection wavelengths were used, respectively: 488 nm and 500–555 nm for eGFP4, roGFP2, and ER tracker green; 561 nm and 615–676 nm for FM4-64, mRFP, and ER tracker red; 405 and 425–460 for aniline blue.

For application of FM4-64 or BFA, the roots of the plants were cut and transferred to liquid 0.5× MS containing 1 μM FM4-64 (Thermo Fisher Scientific) for 20 min and/or 50 μM BFA (Sigma-Aldrich) for 1 h. For ER staining, the roots of plants were transferred to liquid 0.5× MS containing 0.5 μM ER-Tracker Green (glibenclamide BODIPY FL, Thermo Fisher Scientific) or 1 μM ER-Tracker Red (glibenclamide BODIPY TR, Thermo Fisher Scientific) for 1 min. For cell plate staining, seedlings were transferred to 150 mM K_2HPO_4 pH 9.5 containing 0.01% (w/v) aniline blue for 15 min.

For colocalization analysis, at least 10 primary roots were analyzed for each experiment. CLSM images taken in two separate channels were used for colocalization analysis with FIJI software (Schindelin et al., 2012). Particular regions of the image were selected from masks created by using Colocalization Finder tool for colocalization analysis when indicated. The Colocalization Threshold and Coloc2 plugins were used to automate image thresholds and to quantify the Manders and Pearson (r) coefficients between the two channels in the selected region, with the former expressed as colocalization percentage (Manders et al., 1993; Costes et al., 2004).

Ratiometric Fluorescence Imaging

Roots of 10-d-old pGGZUBI10:UPS5L-roGFP2/wild type or pGGZUBI10:UPS5L-roGFP2/wild-type plants grown in 0.5× MS 1% (w/v) agar vertical plates were used for ReTA (redox-based topology analysis) experiments. Ratiometric confocal imaging was performed on an Olympus FV1200 laser scanning microscope with a 60× oil-immersion objective lens. roGFP fluorescence was excited at 405 and 488 nm and collected using a band-pass filter at 485–545 nm. Ratiometric analysis of nonsaturated images was performed using FIJI software (Schindelin et al., 2012). After background subtraction, Gaussian and Median filters were applied to both images. The 405-nm image was divided by the 488-nm image, and the ratio images were illustrated using the "Thermal" LUT setting pixel values between 0 (reduced) and 3 (oxidized). At least four independent lines for each construction were analyzed. Plants expressing free cytosolic (GRX1-roGFP2) or ER (roGFP2-HDEL) roGFP2 were used as controls (Meyer et al., 2007; Brach et al., 2009).

Data Analysis and Statistics

The Infostat software version 2018 and Graph Pad Prism 7 were used for statistical analysis. The normality and homogeneity of variance were tested by Shapiro-Wilk's and Levene's, respectively. For comparison of data with parametric distribution ANOVA followed by DGC′ test (Di Rienzo, Guzmán y Casanoves method) were performed (Di Rienzo et al., 2002). For comparison of data with nonparametric distribution Kruskal-Wallis followed by Dunn's test were performed. Statistically significant differences ($P < 0.05$) are reported in the text.

Accession Numbers

Sequence data from this article can be found in the GenBank/EMBL data libraries under accession numbers NP_565303.1 (AtUPS1), NP_849708.1 (AtUPS5L), and NP_564246.1 (AtUPS5S).

Supplemental Data

The following supplemental materials are available.

Supplemental Figure S1. Functional complementation of a yeast mutant deficient in uracil uptake with AtUPS1-eGFP4.

Supplemental Figure S2. Expression of *AtUPS5* transcripts in UPS5L-eGFP4 and UPS5S-mRFP transgenic lines.

Supplemental Figure S3. Colocalization of UPS5L and UPS5S with ER-trackers.

Supplemental Figure S4. Subcellular localization of UPS5L::roGFP2 and UPS5S:roGFP in *Nicotiana benthamiana*.

Supplemental Figure S5. Subcellular localization of UPS5 in the cell plate.

Supplemental Figure S6. Subcellular localization of UPS5S:FP and FM4-64 in the endomembrane compartments.

Supplemental Figure S7. Phenotype of independent transgenic lines of UPS5L-eGFP4 and UPS5S-mRFP grown with allantoin as N source.

Supplemental Figure S8. Germination rate of UPS5L-eGFP4 and UPS5S-mRFP grown with allantoin as N source.

Supplemental Figure S9. Shoot allantoin content of UPS5L-eGFP4 and UPS5S-mRFP lines after incubation with allantoin.

Supplemental Figure S10. Response of independent lines of UPS5L-eGFP4 and UPS5S-mRFP lines to salt stress.

Supplemental Figure S11. Response of UPS5L-eGFP4 and UPS5S-mRFP lines to salt stress and allantoin.

Supplemental Figure S12. Allantoin content and response of *ups5-1* lines to salt stress.

Supplemental Table S1. Plasmids used and generated in this work.

Supplemental Table S2. List of oligonucleotides used in this work

Supplemental Table S3. Ct y ΔCt values used for expression analysis of *AtUPS5* splicing variants under salt stress.

ACKNOWLEDGMENTS

We thank Dr. Rainer Waadt and Dr. Falco Krüger (Center for Organismal Studies, Heidelberg, Germany) for microscopy assistance. The authors greatly acknowledge the technical and imaging assistance of Dr. Carlos Mas from the Centro de Micro y Nanoscopía de Córdoba, -CEMINCO- CONICET-Universidad Nacional de Córdoba, Córdoba, Argentina. The authors also gratefully acknowledge Dr. Marcos Carpio and Dr. César Prucca (CIQUIBIC-CONICET, Córdoba, Argentina) for providing the ER trackers. We thank to Dr. Maria Elena

Alvarez, Dr. Nicolás Cecchini, and other colleagues from CIQUIBIC-CONICET (FCQ-UNC) who provided insight and expertise that greatly assisted the research.

Received November 22, 2019; accepted December 12, 2019; published December 20, 2019.

LITERATURE CITED

Brach T, Soyk S, Müller C, Hinz G, Hell R, Brandizzi F, Meyer AJ (2009) Non-invasive topology analysis of membrane proteins in the secretory pathway. Plant J **57:** 534–541

Brychkova G, Alikulov Z, Fluhr R, Sagi M (2008) A critical role for ureides in dark and senescence-induced purine remobilization is unmasked in the Atxdh1 Arabidopsis mutant. Plant J **54:** 496–509

Casartelli A, Melino VJ, Baumann U, Riboni M, Suchecki R, Jayasinghe NS, Mendis H, Watanabe M, Erban A, Zuther E, et al (2019) Opposite fates of the purine metabolite allantoin under water and nitrogen limitations in bread wheat. Plant Mol Biol **99:** 477–497

Clough SJ, Bent AF (1998) Floral dip: A simplified method for *Agrobacterium*-mediated transformation of *Arabidopsis thaliana*. Plant J **16:** 735–743

Collier R, Tegeder M (2012) Soybean ureide transporters play a critical role in nodule development, function and nitrogen export. Plant J **72:** 355–367

Costes SV, Daelemans D, Cho EH, Dobbin Z, Pavlakis G, Lockett S (2004) Automatic and quantitative measurement of protein-protein colocalization in live cells. Biophys J **86:** 3993–4003

Desimone M, Catoni E, Ludewig U, Hilpert M, Schneider A, Kunze R, Tegeder M, Frommer WB, Schumacher K (2002) A novel superfamily of transporters for allantoin and other oxo derivatives of nitrogen heterocyclic compounds in Arabidopsis. Plant Cell **14:** 847–856

Dettmer J, Hong-Hermesdorf A, Stierhof Y-D, Schumacher K (2006) Vacuolar H+-ATPase activity is required for endocytic and secretory trafficking in Arabidopsis. Plant Cell **18:** 715–730

Di Rienzo JA, Guzman AW, Casanoves F (2002) A multiple-comparisons method based on the distribution of the root node distance of a binary tree. J Agr Biol Envir St **7:** 129–142

Froissard M, Belgareh-Touzé N, Buisson N, Desimone M, Frommer WB, Haguenauer-Tsapis R (2006) Heterologous expression of a plant uracil transporter in yeast: Improvement of plasma membrane targeting in mutants of the Rsp5p ubiquitin protein ligase. Biotechnol J **1:** 308–320

Gus'kov E, Kletskii M, Kornienko I, Olekhnovich L, Chistyakov V, Shkurat T, Prokof'Ev V, Zhdanov YA (2002) Allantoin as a free-radical scavenger. Dokl Biochem Biophys **383:** 105–108

Hesberg C, Hänsch R, Mendel RR, Bittner F (2004) Tandem orientation of duplicated xanthine dehydrogenase genes from *Arabidopsis thaliana*: Differential gene expression and enzyme activities. J Biol Chem **279:** 13547–13554

Irani S, Todd CD (2016) Ureide metabolism under abiotic stress in *Arabidopsis thaliana*. J Plant Physiol **199:** 87–95

Irani S, Todd CD (2018) Exogenous allantoin increases Arabidopsis seedlings tolerance to NaCl stress and regulates expression of oxidative stress response genes. J Plant Physiol **221:** 43–50

Kader MA, Lindberg S (2010) Cytosolic calcium and pH signaling in plants under salinity stress. Plant Signal Behav **5:** 233–238

Kanani H, Dutta B, Klapa MI (2010) Individual vs. combinatorial effect of elevated CO_2 conditions and salinity stress on *Arabidopsis thaliana* liquid cultures: Comparing the early molecular response using time-series transcriptomic and metabolomic analyses. BMC Syst Biol **4:** 177

Lamberto I, Percudani R, Gatti R, Folli C, Petrucco S (2010) Conserved alternative splicing of Arabidopsis transthyretin-like determines protein localization and S-allantoin synthesis in peroxisomes. Plant Cell **22:** 1564–1574

Lampropoulos A, Sutikovic Z, Wenzl C, Maegele I, Lohmann JU, Forner J (2013) GreenGate - a novel, versatile, and efficient cloning system for plant transgenesis. PLoS ONE **8:** e83043

Lee KH, Piao HL, Kim H-Y, Choi SM, Jiang F, Hartung W, Hwang I, Kwak JM, Lee I-J, Hwang I (2006) Activation of glucosidase via stress-induced polymerization rapidly increases active pools of abscisic acid. Cell **126:** 1109–1120

Lescano CI, Martini C, González CA, Desimone M (2016) Allantoin accumulation mediated by allantoinase downregulation and transport by Ureide Permease 5 confers salt stress tolerance to Arabidopsis plants. Plant Mol Biol **91:** 581–595

Luo Y, Scholl S, Doering A, Zhang Y, Irani NG, Rubbo SD, Neumetzler L, Krishnamoorthy P, Van Houtte I, Mylle E, et al (2015) V-ATPase activity in the TGN/EE is required for exocytosis and recycling in Arabidopsis. Nat Plants **1:** 15094

Manders EMM, Verbeek FJ, Aten JA (1993) Measurement of co-localization of objects in dual-colour confocal images. J Microsc **169:** 375–382

McClure PR, Israel DW (1979) Transport of nitrogen in the xylem of soybean plants. Plant Physiol **64:** 411–416

Meyer AJ, Brach T, Marty L, Kreye S, Rouhier N, Jacquot JP, Hell R (2007) Redox-sensitive GFP in Arabidopsis thaliana is a quantitative biosensor for the redox potential of the cellular glutathione redox buffer. Plant J **52:** 973–986

Michniewicz M, Zago MK, Abas L, Weijers D, Schweighofer A, Meskiene I, Heisler MG, Ohno C, Zhang J, Huang F, et al (2007) Antagonistic regulation of PIN phosphorylation by PP2A and PINOID directs auxin flux. Cell **130:** 1044–1056

Miller G, Suzuki N, Ciftci-Yilmaz S, Mittler R (2010) Reactive oxygen species homeostasis and signalling during drought and salinity stresses. Plant Cell Environ **33:** 453–467

Mineyuki Y, Gunning B (1990) A role for preprophase bands of microtubules in maturation of new cell walls, and a general proposal on the function of preprophase band sites in cell division in higher plants. J Cell Sci **97:** 527–537

Nikiforova VJ, Kopka J, Tolstikov V, Fiehn O, Hopkins L, Hawkesford MJ, Hesse H, Hoefgen R (2005) Systems rebalancing of metabolism in response to sulfur deprivation, as revealed by metabolome analysis of Arabidopsis plants. Plant Physiol **138:** 304–318

Nourimand M, Todd CD (2016) Allantoin increases cadmium tolerance in Arabidopsis via activation of antioxidant mechanisms. Plant Cell Physiol **57:** 2485–2496

Nourimand M, Todd CD (2019) There is a direct link between allantoin concentration and cadmium tolerance in Arabidopsis. Plant Physiol Biochem **135:** 441–449

Pélissier HC, Frerich A, Desimone M, Schumacher K, Tegeder M (2004) PvUPS1, an allantoin transporter in nodulated roots of French bean. Plant Physiol **134:** 664–675

Pfaffl MW 2004. Quantification strategies in real-time PCR. In: Bustin SA, ed. AZ of Quantitative PCR. 3. La Jolla, California: International University Line, p 89–113.

Rose MT, Rose TJ, Pariasca-Tanaka J, Yoshihashi T, Neuweger H, Goesmann A, Frei M, Wissuwa M (2012) Root metabolic response of rice (*Oryza sativa* L.) genotypes with contrasting tolerance to zinc deficiency and bicarbonate excess. Planta **236:** 959–973

Sagi M, Omarov RT, Lips SH (1998) The Mo-hydroxylases xanthine dehydrogenase and aldehyde oxidase in ryegrass as affected by nitrogen and salinity. Plant Sci **135:** 125–135

Schindelin J, Arganda-Carreras I, Frise E, Kaynig V, Longair M, Pietzsch T, Preibisch S, Rueden C, Saalfeld S, Schmid B, et al (2012) Fiji: An open-source platform for biological-image analysis. Nat Methods **9:** 676–682

Schmidt A, Baumann N, Schwarzkopf A, Frommer WB, Desimone M (2006) Comparative studies on ureide permeases in *Arabidopsis thaliana* and analysis of two alternative splice variants of AtUPS5. Planta **224:** 1329–1340

Schmidt A, Su Y-H, Kunze R, Warner S, Hewitt M, Slocum RD, Ludewig U, Frommer WB, Desimone M (2004) UPS1 and UPS2 from Arabidopsis mediate high affinity transport of uracil and 5-fluorouracil. J Biol Chem **279:** 44817–44824

Schwacke R, Schneider A, van der Graaff E, Fischer K, Catoni E, Desimone M, Frommer WB, Flügge U-I, Kunze R (2003) ARAMEMNON, a novel database for Arabidopsis integral membrane proteins. Plant Physiol **131:** 16–26

Schwarzländer M, Fricker MD, Müller C, Marty L, Brach T, Novak J, Sweetlove LJ, Hell R, Meyer AJ (2008) Confocal imaging of glutathione redox potential in living plant cells. J Microsc **231:** 299–316

Serventi F, Ramazzina I, Lamberto I, Puggioni V, Gatti R, Percudani R (2010) Chemical basis of nitrogen recovery through the ureide pathway: Formation and hydrolysis of S-ureidoglycine in plants and bacteria. ACS Chem Biol **5:** 203–214

Shen J, Zeng Y, Zhuang X, Sun L, Yao X, Pimpl P, Jiang L (2013) Organelle pH in the Arabidopsis endomembrane system. Mol Plant **6:** 1419–1437

Simon S, Skůpa P, Viaene T, Zwiewka M, Tejos R, Klíma P, Čarná M, Rolčík J, et al (2016) PIN6 auxin transporter at endoplasmic reticulum and plasma membrane mediates auxin homeostasis and organogenesis in Arabidopsis. New Phytol **211:** 65–74

Soltabayeva A, Srivastava S, Kurmanbayeva A, Bekturova A, Fluhr R, Sagi M (2018) Early senescence in older leaves of low nitrate-grown Atxdh1 uncovers a role for purine catabolism in N supply. Plant Physiol **178:** 1027–1044

Stamm S, Ben-Ari S, Rafalska I, Tang Y, Zhang Z, Toiber D, Thanaraj TA, Soreq H (2005) Function of alternative splicing. Gene **344:** 1–20

Todd CD, Tipton PA, Blevins DG, Piedras P, Pineda M, Polacco JC (2005) Update on ureide degradation in legumes. J Exp Bot **57:** 5–12

Ventura Y, Myrzabayeva M, Alikulov Z, Omarov R, Khozin-Goldberg I, Sagi M (2014) Effects of salinity on flowering, morphology, biomass accumulation and leaf metabolites in an edible halophyte. AoB Plants **6:** plu053

Vernon LP (1960) Spectrophotometric determination of chlorophylls and pheophytins in plant extracts. Anal Chem **32:** 1144–1150

Vogels GD, Van Der Drift C (1970) Differential analyses of glyoxylate derivatives. Anal Biochem **33:** 143–157

Wang P, Kong C-H, Sun B, Xu X-H (2012) Distribution and function of allantoin (5-ureidohydantoin) in rice grains. J Agric Food Chem **60:** 2793–2798

Watanabe S, Matsumoto M, Hakomori Y, Takagi H, Shimada H, Sakamoto A (2014) The purine metabolite allantoin enhances abiotic stress tolerance through synergistic activation of abscisic acid metabolism. Plant Cell Environ **37:** 1022–1036

Werner AK, Medina-Escobar N, Zulawski M, Sparkes IA, Cao F-Q, Witte C-P (2013) The ureide-degrading reactions of purine ring catabolism employ three amidohydrolases and one aminohydrolase in Arabidopsis, soybean, and rice. Plant Physiol **163:** 672–681

Werner AK, Romeis T, Witte C-P (2010) Ureide catabolism in *Arabidopsis thaliana* and *Escherichia coli*. Nat Chem Biol **6:** 19–21

Werner AK, Witte C-P (2011) The biochemistry of nitrogen mobilization: Purine ring catabolism. Trends Plant Sci **16:** 381–387

Wormit A, Traub M, Flörchinger M, Neuhaus HE, Möhlmann T (2004) Characterization of three novel members of the *Arabidopsis thaliana* equilibrative nucleoside transporter (ENT) family. Biochem J **383:** 19–26

Zrenner R, Stitt M, Sonnewald U, Boldt R (2006) Pyrimidine and purine biosynthesis and degradation in plants. Annu Rev Plant Biol **57:** 805–836